Density functional theory of freezing for binary mixtures of 2D superparamagnetic colloids

Manjori Mukherjee[1], Pankaj Mishra[1] and Hartmut Löwen[2]

[1] Department of Applied Physics, Indian School of Mines, Dhanbad-826004, Jharkhand, India
[2] Institut für Theoretische Physik II, Heinrich-Heine-Universität, Universitätsstraße 1, D-40225 Düsseldorf, Germany

E-mail: mpankajg@gmail.com

Abstract

Density functional theory of freezing is used to study the phase diagram of a binary mixture of superparamagnetic colloidal particles in two dimensions. The particles interact via a purely repulsive potential that scales as the inverse cube of the inter-particle separation.
This corresponds to a magnetic dipole interaction where the dipoles are induced by an external magnetic field applied normal to the plane. The pair correlation functions needed as input information in the density functional theory are calculated by the hypernetted chain integral equation closure. Considering the freezing into a disordered triangular solid phase, a spindle phase diagram is found for the susceptibility ratio 0.9 of the species, which changes to an azeotrope at a ratio 0.8. A eutectic-like phase diagram with an intervening solid phase emerges for the susceptibility ratio 0.7. The results are verifiable in real-space experiments on superparamagnetic colloids in external magnetic fields.

Keywords: theory and models of liquid structure, colloids, solid–liquid transition

(Some figures may appear in colour only in the online journal)

1. Introduction

Binary mixtures can exhibit rich equilibrium phase diagrams including eutectic, azeotropic, and spindle shapes as a function of composition, together with compound solids with various compositions of the two species [1–6]. Therefore, binary systems provide an ideal testbed for solidification and vitrification processes, including homogeneous and heterogeneous nucleation and crystal growth [7, 8]. For one-component systems, on the other hand, the situation is much simpler as there are typically only very few stable solid structures.

Recent studies have used two spatial dimensions with a repulsive dipole–dipole interaction between the particles. This interaction is motivated from superparamagnetic colloidal particles at a pending air-water interface in an external magnetic field. The latter induces dipole moments in the particles according to their magnetic susceptibility. These superparamagnetic suspensions are very good realizations of a

classical 2D repulsive dipole–dipole system [9–14]. Recently, for a one-component system, a density functional approach was put forward to calculate the freezing transition [15, 16]. This density functional approach was made dynamical to explore crystal nucleation and subsequent growth phenomena at imposed nucleation clusters [17–19]. Two-component dipolar systems can also be prepared and were studied experimentally [20–25], however, the full parameter space in equilibrium now also involves the composition and the susceptibility ratio, which sets the relative interaction strength. The zero-temperature phase diagram of the binary system has been explored over a wide range of susceptibility ratios, and a wealth of stable solid lattices were found [26] (see also [27]).

Here, we generalize the density functional theory in terms of a two-component dipolar system, using the binary fluid pair structure as an input. The latter is obtained within the hypernetted chain liquid integral theory [28]. We calculate the equilibrium freezing phase diagram for finite temperature and

a given fixed susceptibility ratio. Increasing the asymmetry, the phase diagram shifts from a spindle-type towards an azeotropic-type and, finally, to a eutectic-type. While this trend is in general qualitatively agrees with results obtained for other mixtures of repulsive particles in two and three dimensions, the eutectic phase diagram obtained here has an unusual topology involving an intervening solid phase. Moreover, the proposed density functional can serve as a building block for future dynamical studies of nucleation and growth, similar to [17–19] that for the one-component system.

The paper is organized as follows: We describe our model in detail in section 2 and in section 3, we discuss the details of liquid integral equation theory. The density functional theory employed to study the freezing transition and the common tangent method is given in section 4. We discuss the resulting phase diagrams in section 5 and provide conclusions in section 6.

2. The model

We study the freezing in a two-component mixture of a model 2D fluid containing superparamagnetic colloidal particles aligned perpendicularly to the 2D-plane by an external magnetic field. Each component is characterized by its partial density ρ_i and susceptibility χ_i ($i = 1, 2$). We model the particles as point-like but refer to the particles having larger susceptibility as 'big' (species 1, A particle) and those with smaller susceptibility as 'small'; (species 2, B particle). The particles are exposed to an external static magnetic field $\mathbf{B}$ that induces a magnetic moment $\mathbf{M_i} = \chi_i \mathbf{B}$ ($i = 1, 2$) in the particles. The strength of the induced dipole moment can be conveniently tuned by the magnitude of the external magnetic field. The effective interaction between particles through their induced parallel dipole moments thus turns out to be purely repulsive and soft. The three different interactions among particles pairs are

$$u_{ij}(r) = \frac{\mu_0}{4\pi} \frac{\mathbf{M_i M_j}}{r_{ij}^3}; \qquad i, j = 1, 2, \qquad (2.1)$$

where μ_0 is the vacuum permeability and r_{ij} is the interparticle separations. We define the average interparticle distance $a = 1/\sqrt{\rho}$ with $\rho = \rho_1 + \rho_2$ as characteristic length scale of the system and introduce the dimensionless coupling strengths Γ_{ij}, expressed as

$$\Gamma_{ij} = \frac{\mu_0}{4\pi} \frac{\beta \chi_i \chi_j \mathbf{B}^2}{a^3}; \qquad i, j = 1, 2, \qquad (2.2)$$

where $\beta = 1/k_B T$, with k_B being Boltzmann's constant and T as the temperature. Using the definition in equation (2.2) and rescaling the inter-particle distances with the characteristic average distance a, $x = r_{ij}/a$, we can write the interaction (2.1) in the form

$$\beta u_{ij}(x) = \frac{\Gamma_{ij}}{x^3} \qquad (2.3)$$

Therefore, the two-component system can be completely characterized by three parameters:

1 the composition defined as $\gamma_1 = \rho_1/\rho$, or complementarily as $\gamma_2 = 1 - \gamma_1$.

2 the susceptibility ratio $m = \chi_2/\chi_1$, which we call the susceptibility asymmetry parameter,

3 one of the three interaction strengths Γ_{ij}, which we chose to be Γ_{11}. Then, the two remaining coupling strength parameters are $\Gamma_{12} = m\Gamma_{11}$ and $\Gamma_{22} = m^2\Gamma_{11}$. Γ_{11} can be expressed in terms of the dimensionless scaled density ρ^* and temperature t^* as

$$\Gamma_{11} = \frac{(\rho^*)^{3/2}}{t^*} \qquad (2.4)$$

where $\rho^* = \ell^2 \rho$ and $t^* = k_B T/\epsilon$. Here, $\ell = (\mu_0 \chi_1/4\pi)^{1/3}$ is the natural length scale and $\epsilon = \chi_1 \mathbf{B}^2$ is the natural energy scale originating from the interaction potential $u_{11}(r)$.

As previously mentioned, the zero temperature phase diagram as a function of composition and susceptibility asymmetry for the above system has been explored by Assoud *et al* [26]. Using lattice sums, a rich variety of different crystalline structures was reported to be stable, including $A_m B_n$ structures with triangular, square, rectangular, and rhombic lattices, with a basis comprising various structures of A and B particles. For smaller susceptibility asymmetry, stable intermediate AB_2 and A_2B crystals besides A and B triangular crystals were found. Here, we consider pure triangular A, pure triangular B, and substitutionally disordered triangular solid (DS) phases as the candidate structures, and density functional theory is used to study the freezing transitions. We restrict our study to substitutionally disordered solids as density functional theory is expected to be most accurate, and simulation data is missing in this case.

3. Liquid integral equation theory

The pair structure in the mixture is fully determined by the set of partial radial distribution functions $g_{ij}(r)$ or the direct correlation functions $c_{ij}(r)$. Defining the total pair correlation function $h_{ij}(r) = g_{ij}(r) - 1$, the former two quantities are connected via the Ornstein–Zernike (OZ) relation [29]

$$h_{ij}(r_{12}) = c_{ij}(r_{12}) + \rho \sum_l \gamma_l \int dr_3 c_{il}(r_{13}) h_{lj}(r_{32}) \qquad (3.1)$$

Since the OZ equation couples two unknown quantities, $h_{ij}(r)$ and $c_{ij}(r)$, it must be supplemented with a closure relationship between these functions. The HNC closure relation for the mixture can be written as [29]

$$h_{ij}(x) = \exp[-\beta u_{ij}(x) + h_{ij}(x) - c_{ij}(x)] - 1 \qquad (3.2)$$

The pair correlation functions are obtained by the self-consistent solution of equations (3.1) and (3.2). To solve the OZ equation, it is advisable to use its Fourier representation, which is obtained by substituting the Fourier–Bessel transform of h and c functions in equation (3.1). The Fourier–Bessel transform of a general function $f(r)$ in 2D is defined as [30, 31]

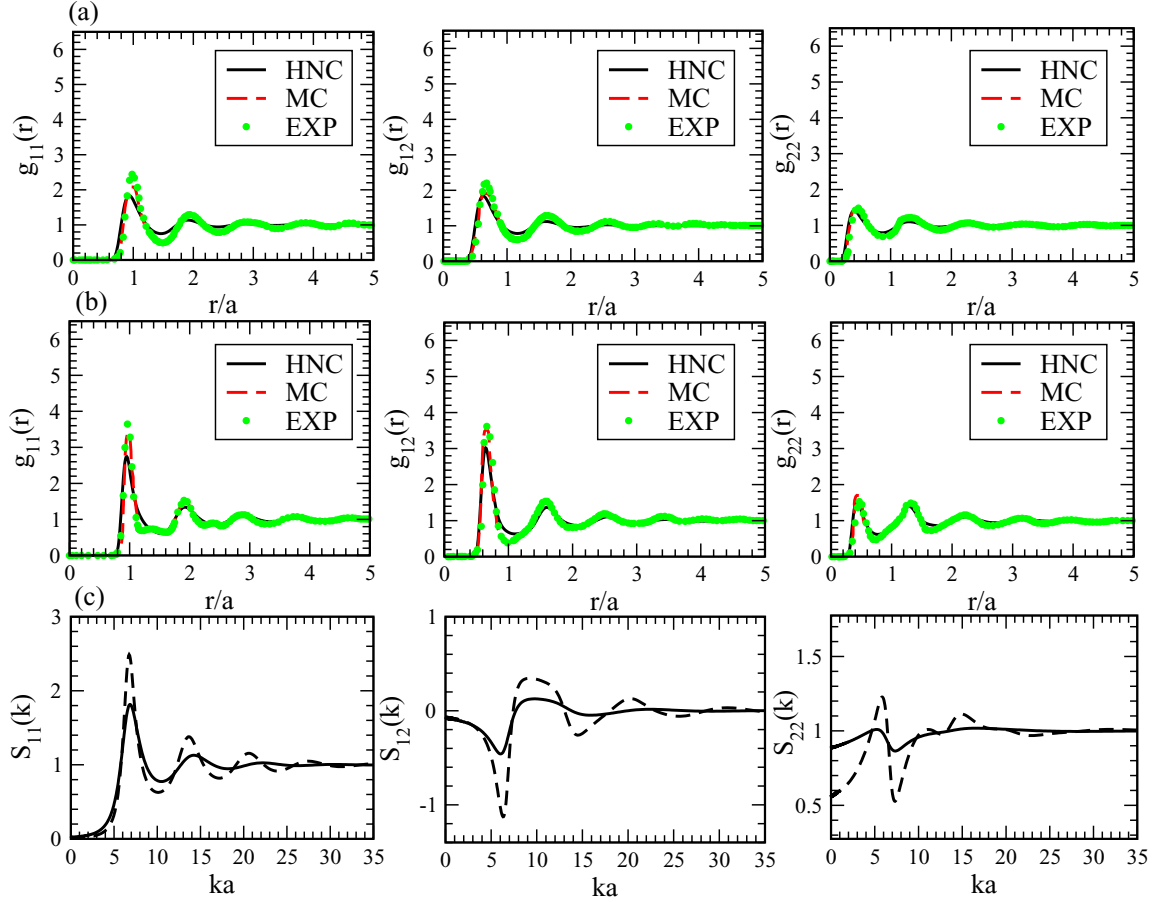$$f(k) = 2\pi \int_0^\infty dr\, r f(r) J_n(kr) \qquad (3.3)$$

Figure 1. Comparison of partial radial distribution functions $g_{11}(r)$, $g_{12}(r)$, and $g_{22}(r)$ for parameters (*a*) $\gamma_2 = 0.29$, $\Gamma_{11} = 4.9$ and (*b*) $\gamma_2 = 0.44$, $\Gamma_{11} = 22.6$, at fixed susceptibility ratio $m = 0.1$, with the corresponding experimental and Monte–Carlo simulation results of Assoud *et al* [32]. (*c*) shows the three partial structure factors versus wave number k as obtained from the HNC closure. The full lines are for parameters of (*a*) and the dashed lines for the parameters of (*b*).

$$f(r) = \frac{2\pi}{(2\pi)^2} \int_0^\infty \mathrm{d}k\, k f(k) J_n(kr) \qquad (3.4)$$

where $J_n(kr)$ is the Bessel function of first kind of *n*th order. Substituting $h(r)$ and $c(r)$ by their respective Fourier transforms in equation (3.1), we get a set of algebraic equations in Fourier space

$$h_{ij}(k) = c_{ij}(k) + \rho \sum_l \gamma_l c_{il}(k) h_{lj}(k) \qquad (3.5)$$

Due to symmetry of the potentials, $h_{12} = h_{21}$. Therefore, the pair structure is fully determined by three correlation functions h_{11}, h_{12}, and h_{22}. These are calculated by solving equations (3.5) and (3.2) iteratively at a grid of interaction strength Γ_{11} for different compositions and susceptibility ratio χ_2/χ_1. In figure 1, we compare our results of partial radial distribution functions $g_{ij}(r)$ with those of Assoud *et al* [32], obtained by experiment and Monte–Carlo simulation. Results are compared for a mixture of highly asymmetric particles with ratio $\chi_2/\chi_1 = 0.1$, with (a) composition $\gamma_2 = 0.29$, coupling strength $\Gamma_{11} = 4.9$ and (b) $\gamma_2 = 0.44$, $\Gamma_{11} = 22.6$. Though the peak amplitude is slightly underestimated, the HNC integral equation theory is in good agreement with experimental and simulation results. Finally, figure 1 also shows the three partial

structure factors for the corresponding parameter combinations as obtained from the HNC theory, which directly enter into the density functional as discussed in the next section[3].

4. Density functional theory and freezing transitions

Density functional theory (DFT) provides a general mean to approximate the Helmholtz free energy using known structural and thermodynamic information for the corresponding uniform fluid. DFT can be extensively formulated and applied for the study of freezing transitions in one-component as well as two-component systems [33–42, 47, 49–51]. Here, we apply the Ramakrishnan–Yussouff (RY) [52] approximation to explore the phase behaviour of our system. The RY-approximation requires a pair correlation of a bulk reference fluid as an input and thereby, the results depend on the approximation used to calculate these input quantities. In the one-component case and for very long-ranged interaction in two dimensions, it has indeed been shown that the results are affected by quality of the structural input [53].

---

[3] Here, the structure is slightly underestimated by the HNC closure used. This is expected to cause a slight shift of the freezing line towards higher temperatures but a quantitative estimate of this shift is difficult to achieve.

The reduced Helmholtz free energy functional $\mathcal{F}[\rho]$ of an inhomogeneous system is a functional of single particle density distribution $\rho(r)$ and is written for a two component system as

$$\mathcal{F}[\{\rho_\nu(\mathbf{r})\}] = \mathcal{F}_{id}[\{\rho_\nu(\mathbf{r})\}] + \mathcal{F}_{ex}[\{\rho_\nu(\mathbf{r})\}], \quad \nu = 1, 2 \tag{4.1}$$

The ideal gas part is exactly known and written for a two-component system as

$$\beta\mathcal{F}_{id}[\{\rho_\nu(\mathbf{r})\}] = \sum_{\nu=1}^{2} \int d\mathbf{r}\,\rho_\nu(\mathbf{r})\{\ln[\rho_\nu(\mathbf{r})\lambda_\nu^2] - 1\} \tag{4.2}$$

with $\beta = 1/k_B T$ and λ_ν as the thermal de Broglie wavelength of the νth component. The excess part that arises due to interparticle interaction is related to the two-particle direct pair correlation function of the fluid $c_{\nu\nu'}^{(2)}(|\mathbf{r}_2 - \mathbf{r}_1|)$ as

$$\beta\mathcal{F}_{ex}^s[\{\rho_\nu(\mathbf{r})\}] = \beta\mathcal{F}_{ex}^f[\{\rho_\nu^0\}] - \frac{1}{2}\sum_{\nu\nu'}\int d\mathbf{r}_1 d\mathbf{r}_2$$
$$\times \Delta\rho_\nu(\mathbf{r}_1)\Delta\rho_{\nu'}(\mathbf{r}_2)c_{\nu\nu'}^{(2)}(|\mathbf{r}_2 - \mathbf{r}_1|) \tag{4.3}$$

Here, $\beta\mathcal{F}_{ex}^f[\{\rho_\nu^0\}]$ is the excess free energy density of a homogeneous fluid at uniform density distribution $\{\rho_\nu^0\}$ and $\Delta\rho_\nu(\mathbf{r}) = \rho_\nu(\mathbf{r}) - \rho_\nu^0$.

The equilibrium one-particle density distribution $\{\rho_\nu\}_{eq}$ of the solid phase is determined by minimizing the total free energy functional $\mathcal{F}[\{\rho_\nu(\mathbf{r})\}]$ with respect to the inhomogeneous one-particle density distribution $\{\rho_\nu\}$. We choose our candidate solid to have a compositionally disordered-triangular structure. We consider a single underlying triangular Bravais lattice, with particles of different species distributed irregularly over the sites with probabilities equal to the respective concentrations. A simple parameterization of solid density is

$$\rho_\nu(\mathbf{r}) = \gamma_\nu \sum_{k=1}^{N} \varphi_\nu(\mathbf{r} - \mathbf{R}_k) \tag{4.4}$$

where $\{\mathbf{R}_k\}$ denotes the set of Bravais lattice vectors of a triangular lattice and φ_ν is a function that describes the average particle density around any lattice site occupied by species ν. With the choice of φ_ν to be a normalized Gaussian centered around the lattice sites, the parameterization in real space takes the form

$$\rho_\nu(\mathbf{r}) = \gamma_\nu \left(\frac{\alpha_\nu^*}{\pi}\right)\sum_{k=1}^{N} \exp[-\alpha_\nu^*|\mathbf{r} - \mathbf{R}_k|^2]; \qquad \nu = 1, 2 \tag{4.5}$$

The scaled *localization parameters* $\alpha_1^*(=\alpha_1 a^2)$ and $\alpha_2^*(=\alpha_2 a^2)$ determine the width of the Gaussians. Increasing α_ν^* leads to enhanced particle localization around the lattice sites. Fourier transform of equation (4.5) leads to the the form of density profile in the reciprocal space as

$$\rho_\nu(\mathbf{r}) = \rho_{\nu s}\left[1 + \sum_{\mathbf{G}\neq0} \mu_{\mathbf{G}}^\nu e^{i\mathbf{G}\cdot\mathbf{r}}\right]; \qquad \nu = 1, 2, \tag{4.6}$$

where $\rho_{\nu s}$ is the average density of the solid with respect to the νth species, $\{\mathbf{G}\}$ is the set of reciprocal lattice vectors, and $\mu_{\mathbf{G}}^\nu$ are the dimensionless Fourier components equal to $e^{-\mathbf{G}^2/4\alpha_\nu^*}$.

Substituting equations (4.5)–(4.6) suitably in equations (4.2) and (4.3) we obtain:

For low $\{\alpha_\nu^*\}$

$$\frac{\beta\mathcal{F}_{id}^s}{N} = \sum_\nu \left[\gamma_\nu(\ln\lambda - 1) + \gamma_\nu\ln\rho_\nu + \frac{\gamma_\nu}{2}\sum_{\mathbf{G}\neq0} e^{-\frac{\mathbf{G}^2}{2\alpha_\nu^*}}\right] \tag{4.7}$$

For high $\{\alpha_\nu^*\}$,

$$\frac{\beta\mathcal{F}_{id}^s}{N} = \sum_\nu \left[\gamma_\nu(\ln\lambda - 1) + \gamma_\nu\ln\rho_\nu + \gamma_\nu(\ln\frac{\alpha_\nu^*}{\pi} - 1)\right] \tag{4.8}$$

For intermediate $\{\alpha_\nu^*\}$,

$$\frac{\beta\mathcal{F}_{id}^s}{N} = \sum_\nu \left[\gamma_\nu(\ln\lambda - 1) + \gamma_\nu\ln\rho_\nu + \gamma_\nu\left(\ln\frac{\alpha_\nu^*}{\pi} - 1\right) + \frac{\gamma_\nu\alpha_\nu^*}{\pi}\right.$$
$$\left.\times \int d\mathbf{r}\,\exp(-\alpha_\nu^*\mathbf{r}^2)\ln\left\{1 + \sum_{k\neq0}\exp(-\alpha_\nu^*(\mathbf{R}_k^2 - 2\mathbf{r}\cdot\mathbf{R}_k))\right\}\right] \tag{4.9}$$

For the homogeneous fluid,

$$\frac{\beta\mathcal{F}_{id}^f}{N} = \sum_\nu \left[\gamma_\nu(\ln\lambda - 1) + \gamma_\nu\ln\rho_\nu\right] \tag{4.10}$$

and

$$\frac{\beta\mathcal{F}_{ex}^s}{N} - \frac{\beta\mathcal{F}_{ex}^f}{N} = -\frac{1}{2}\gamma_A^2\sum_{\mathbf{G}}\exp\left(-\frac{\mathbf{G}^2}{2\alpha_A^*}\right)\hat{c}_{AA}(|\mathbf{G}|)$$
$$-\frac{1}{2}\gamma_B^2\sum_{\mathbf{G}}\exp\left(-\frac{\mathbf{G}^2}{2\alpha_B^*}\right)\hat{c}_{BB}(|\mathbf{G}|)$$
$$-\gamma_A\gamma_B\sum_{\mathbf{G}}\exp\left(-\mathbf{G}^2\left\{\frac{1}{2\alpha_A^*} + \frac{1}{2\alpha_B^*}\right\}\right)\hat{c}_{AB}(|\mathbf{G}|) \tag{4.11}$$

Within RY density functional theory, the excess free energy density $\beta\mathcal{F}_{ex}^f/N$ of the fluid is obtained by integrating the compressibility via

$$\frac{\beta\mathcal{F}_{ex}^f}{N} = \int_0^\rho \left(\frac{\beta P}{\rho} - 1\right)\frac{d\rho}{\rho} \tag{4.12}$$

where

$$\left(\frac{\beta P}{\rho} - 1\right) = -\frac{1}{\rho}\sum_{\nu\nu'}\gamma_\nu\gamma_{\nu'}\int_0^\rho d\rho\,c_{\nu\nu'}(k = 0; \rho) \tag{4.13}$$

The freezing transition is located by determining the thermodynamic state characterized by the equality of the pressure P, reduced temperature t^*, and chemical potentials of solid (μ_s^i) and fluid (μ_f^i). The step-by-step procedure to determine the phase diagram is as follows: Equation (4.1) is minimized with respect to the localization parameters α_1^* and α_2^* to get $\beta(\mathcal{F}^s - \mathcal{F}^f)/N$ at a grid of composition γ_B and coupling strength Γ_{11}. Using equation (2.4), the grid of Γ_{11} is then transformed to a density and temperature grid for each composition. We then fix the temperature and integrate equation (4.13) to get the compressibility
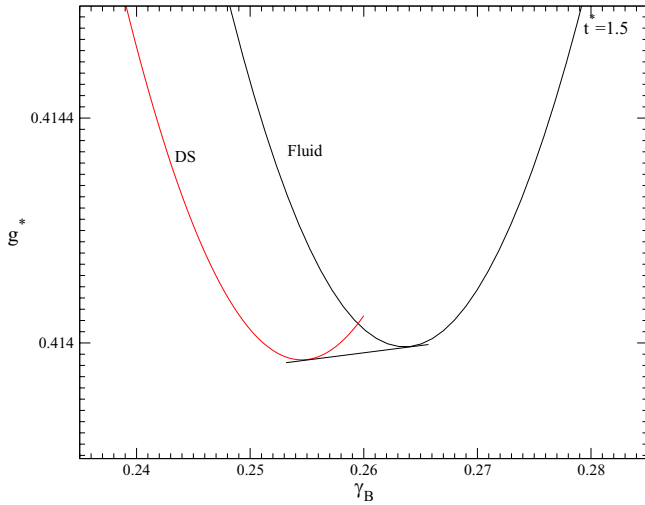
Figure 2. Gibbs free energy versus composition with common tangent construction for a susceptibility ratio 0.9 at a reduced temperature $t^* = 1.5$ and a prescribed pressure $P = 8 \times 10^3 k_B T/\ell^2$. Here, g^* is a shifted Gibbs free energy obtained by subtracting an (irrelevant) linear relation $((\partial g/\partial \gamma_B) \gamma_B + \text{constant})$ passing through two points, one on g_s curve and the other g_f, in order to make the double tangent more visible.

pressure at a grid of density and composition, which, when substituted in equation (4.12), gives the excess free energy contribution of the fluid. By adding the corresponding ideal gas contribution, we get $\beta \mathcal{F}^f/N$ and hence $\beta \mathcal{F}^s/N$. In the case of a disordered solid for which the concentration γ_B is a free variable, the appropriate thermodynamic potential is the Gibbs free energy per particle $g = \mathcal{F}/N + P/\rho$ with pressure $P = \rho^2 \frac{\partial (\mathcal{F}/N)}{\partial \rho}$. The potentials g_s of solid and g_f of fluid are then calculated from the Helmholtz free energy densities. By fixing the pressure at a preassigned value, we interpolate g_s and g_f for all compositions. The coexistence concentrations γ_f and γ_s are then determined by the geometrical common tangent construction, which insures the equality of the chemical potentials in the two phases. The temperature versus composition phase diagram is then obtained by repeating the procedure for various temperatures at the same preassigned pressure.

5. Results

As a result, the phase diagram of the 2D dipolar mixture depends sensitively on the susceptibility ratio χ_2/χ_1. In the present study, we calculate the temperature versus composition phase diagrams for a susceptibility ratio in the range of 0.7 and 1 at a fixed pressure $P = 8 \times 10^3 k_B T/\ell^2$.

5.1. $1 > \chi_2/\chi_1 > 0.85$

In this region, the difference in the susceptibilities of the components of the mixture is small. In figure 2, we plot a representative g versus γ_B curve corresponding to fluid and disordered solid phases at $\chi_2/\chi_1 = 0.90$. We observe that both curves are concave everywhere and intersect only once at a given temperature and pressure. The solid curve $g_s(t^*, P, \gamma_B)$
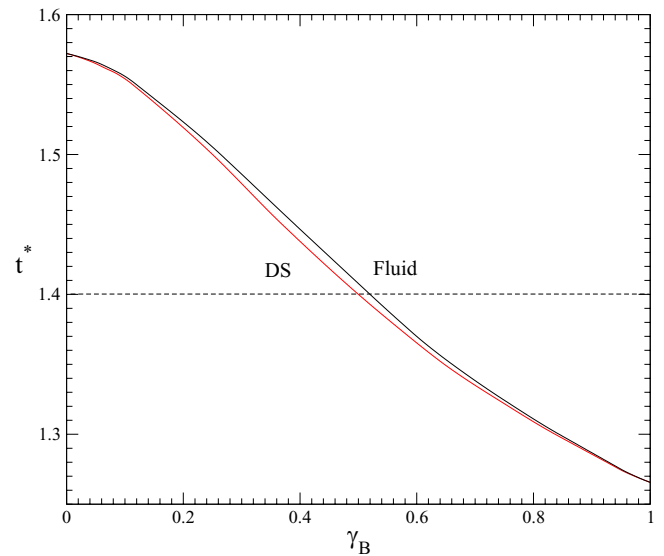

Figure 3. Spindle-type of phase diagram for a susceptibility ratio $\chi_2/\chi_1 = 0.9$ and a prescribed pressure $P = 8 \times 10^3 k_B T/\ell^2$.

falls below $g_f(t^*, P, \gamma_B)$ towards the low γ_B side. The difference in the coexistence compositions of fluid and solid is smaller in the low composition and high composition regions and diminishes at $\gamma_B = 0$ and 1, where triangular crystal of component A and B are stable, respectively. Below $t^* = 1.26$, the solid Gibbs free energy curve moves below the fluid curve for the entire composition but does not intersect it. The resulting phase diagrams corresponding to this range of χ_2/χ_1 values have a *spindle* shape, as shown in figure 3 for $\chi_2/\chi_1 = 0.90$. Therefore, at these asymmetries, the particles are miscible in all proportions in both phases, but the concentration of small particles is always lower in the solid. Note that the solidus and liquidus lines for asymmetry 0.90 are very close to each other, but with clearly visible opening in the middle. At higher susceptibility ratios the two lines shifts closer to each other and hence a spindle looks like a line. A tie line drawn, for example, at $t^* = 1.40$ passes through the disordered solid, coexistence region and the fluid phase as we move along the composition axis.

5.2. $\chi_2/\chi_1 = 0.8$

At $\chi_2/\chi_1 = 0.8$, the g versus γ_B curves are again concave at all temperatures. The solid curve intersects the fluid curve only once up to a certain temperature, below which it intersects twice for a given temperature and pressure. In the composition range lying between the compositions corresponding to the two intersection points, the $g_f(t^*, P, \gamma_B)$ curve drops below $g_s(t^*, P, \gamma_B)$. In figures 4(a)–(c), we show g versus γ_B curve, and the common tangent constructed in the low composition and high composition regions at temperature $t^* = 0.92$. We observe that a temperature $t^* \simeq 0.91$ exists at which the two Gibbs free energy curves have a single point of contact. Further lowering the temperature results in shifting the solid curve below the fluid curve for the entire range of compositions. The resulting phase diagram, shown in figure 5, is an *azeotrope*, with a point corresponding to temperature
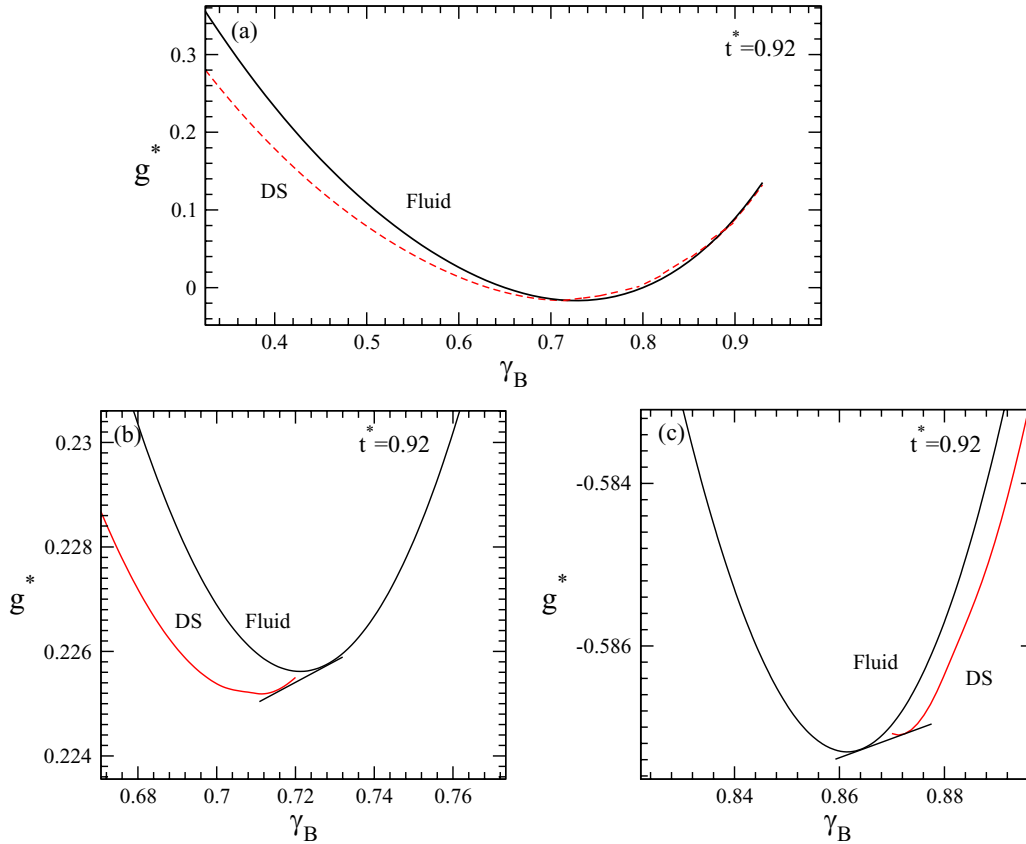
Figure 4. Gibbs free energy versus composition with the corresponding common tangent construction for a susceptibility ratio 0.8 at a reduced temperature of $t^* = 0.92$ and a prescribed pressure $P = 8 \times 10^3 k_B T/\ell^2$.
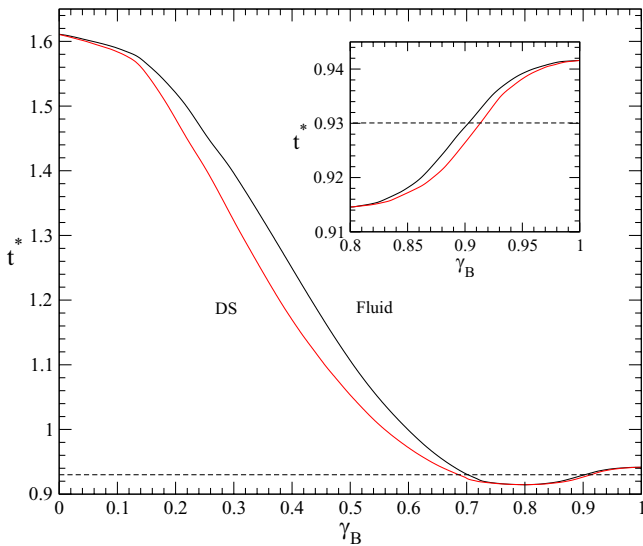

Figure 5. Azeotrope phase diagram for a susceptibility ratio $\chi_2/\chi_1 = 0.8$ with a fluid-disordered solid coexistence line at a reduced temperature of $t^* = 0.92$ and a prescribed pressure $P = 8 \times 10^3 k_B T/\ell^2$. The inset magnifies the regime of high γ_B.

$t^*(t_{az}^*) \simeq 0.91$, where the coexisting phases have identical compositions $\gamma_B \simeq 0.80$. The two components of the mixture are still miscible in the solid phase but at low temperature, the mixture is not ideal. Moving along a tie line drawn at temperature, for example, $t^* = 0.93$ passes through solid

phase, mixed phase, fluid phase, and then again to mixed phase and, finally, to the solid phase in the high composition region.

5.3. $\chi_2/\chi_1 = 0.7$

On further increasing the size asymmetry of the two components of the mixture to 0.7, we observe that, while the fluid Gibbs free energy curve remain concave for the entire range of compositions at all temperatures, the solid curve is found to be concave, lying below the fluid curve and intersecting it only once in the temperature range $1.53 < t^* < 0.88$. Below $t^* = 0.88$, in the temperature range $0.88 < t^* < 0.6$ (see figures 6(*a*)–(*c*)), the solid free energy curve becomes convex for the intermediate compositions, signaling a phase separation into a low composition solid and a high composition solid while intersecting the fluid curve twice, a typical situation for a *eutectic* phase diagram. However, on further lowering the temperature below 0.6, we observe a narrow temperature range extending up to 0.57 in which the two minima of solid shift completely to the left of the fluid curve but free energies of the fluid and solid still intersect twice (see figures 6(*d*)–(*f*)). This leads to a possibility of three common tangents: (i) between the two minima of the solid on the left of the fluid curve, (ii) between the second minimum of solid and the fluid, and (iii) between fluid and the solid curve on the high composition side. Therefore, in this region, a disordered solid (e.g. DSI) coexists with another disordered solid (e.g. DSII) in the low composition side, and the DSII
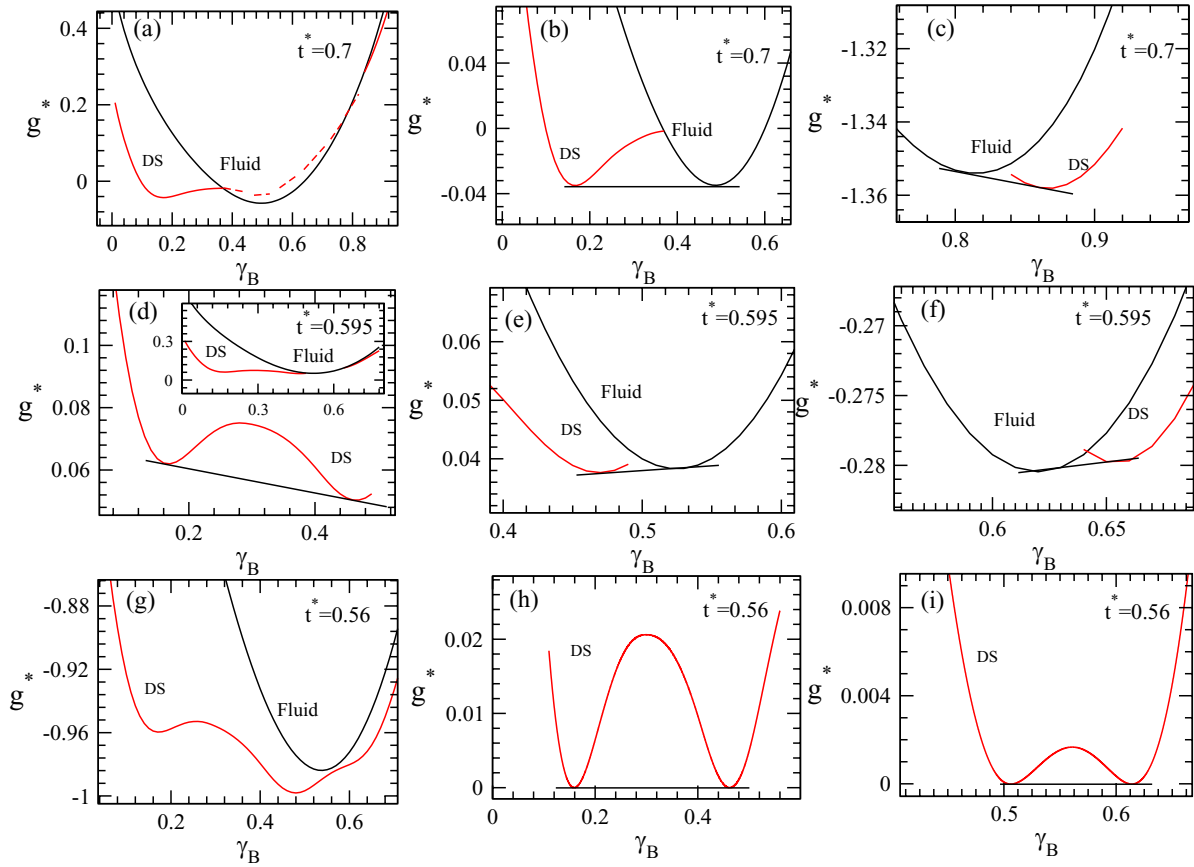
Figure 6. Gibbs free energy versus composition with the common tangent construction for a susceptibility ratio 0.7 at a prescribed pressure $P = 8 \times 10^3 k_B T/\ell^2$. Plots (a)–(c) correspond to $t^* = 0.7$, (d)–(f) correspond to $t^* = 0.595$, and (g)–(i) correspond to $t^* = 0.56$. The inset in (d) shows the same curve on another scale.

coexists with the fluid for the intermediate compositions and fluid coexist again with the solid (e.g. DSIII) in the high composition side. The occurrence of an intervening solid DSII of the same (hexagonal) structure is quite remarkable as this does not occur for other simple pairwise interactions such as hard disks. The intervening stable solid emerges at an almost equimolar composition. Remarkably, such isostructural solid-to-solid transitions also occur in one-component systems for very short-ranged stepwise attractions [43, 44] or repulsions [45, 46] due to competition of two length scales. However, it is not clear whether the mechanism behind isostructural coexistence is the same here.

For temperatures less than 0.57, the solid curve falls below the fluid and does not intersect it (see figures 6(g)–(i)). We notice the presence of an additional minimum towards high composition side in the solid free energy curve, along with the two minima corresponding to DSI and DSII. Therefore, two common tangents can be drawn: (i) between I and II minimum, giving coexistence compositions for DSI and DSII and (ii) between the second and the third minimum, giving coexistence compositions for DSII and DSIII. On further lowering the temperature, the solid free energy data size reduces, which leads initially to the disappearance of the third minimum and then to the second minimum as well.

The resulting phase diagram is shown in figure 7. In the temperature range $t^* \geqslant 0.6$, the phase diagram seems to be
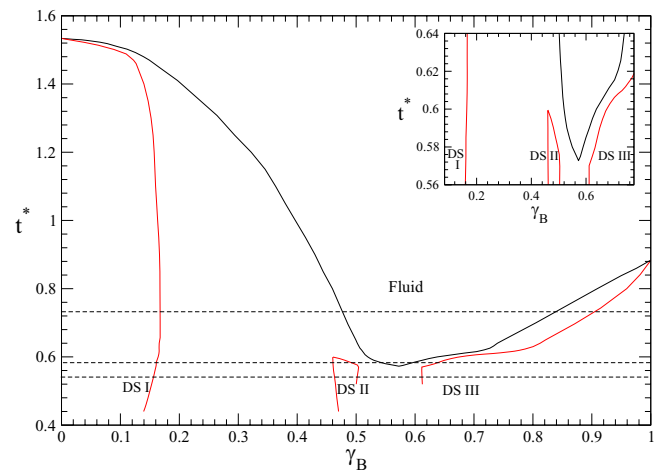

Figure 7. Eutectic phase diagram for $\chi_2/\chi_1 = 0.7$ with the intervening solid phase (DSII). The inset is a magnification close to the eutectic point.

eutectic. A tie line drawn at $t^* = 0.70$ takes us through solid, solid–fluid coexistence region, fluid, fluid–solid coexistence region, and then to the solid on the high composition side. However, for temperature range $0.6 < t^* \lesssim 0.57$, moving along a tie line, we pass through a complex phase sequence, namely DSI, DSI-DSII coexistence region, DSII, DSII-fluid coexistence region, fluid, fluid-DSIII coexistence region, and

finally to the DSIII phase. For temperatures less than 0.57, the intermediate fluid phase disappears.

6. Conclusions

In conclusion, we have proposed a Ramakrishnan–Yussouff-like density functional for binary mixture, with dipolar interactions in two spatial dimensions. The method of common tangent construction is used to determine the phase diagram of the system for fixed susceptibility ratios 0.9, 0.8, and 0.7 of the two species. We obtain a spindle phase diagram at susceptibility ratio 0.9, which changes to an azeotrope at a ratio of 0.8. For a susceptibility ratio of 0.7, a eutectic-like phase diagram with an intervening solid was obtained. These results are qualitatively similar to those obtained for 2D binary hard-disk liquids [48] and 3D hard sphere mixtures [49, 50], but the eutectic phase diagram has an interesting and unusual intervening solid structure, which appears to be specific to the soft repulsive interactions used in our model. These results can, in principle, be confirmed by real-space experiments on superparamagnetic colloidal particles [21] or by Monte–Carlo computer simulations, see e.g. [54].

Future work should be focused on the dynamics of crystallization for which dynamical density functional theory was developed [55–57]. For a recent application to 2D binary mixtures, see [58]. Thereby, our equilibrium functional can be used to access the fascinating crystal nucleation and growth of binary colloidal crystals from the melt. It further provides a microscopic basis to numerically derive more efficient phase-field-crystal models [59, 60] for mixtures. Another line of future research concerns equilibrium density functional studies of non-spherical particles [61] such as spherocylinders [62], dumbbells [63], cubes [64, 65], and polyhedra [66] for which the freezing behaviour of mixtures is hardly understood.

Acknowledgments

References

[1] Meller A and Stavans J 1992 *Phys. Rev. Lett.* **68** 3645
[2] Hunt W J and Zukoski C F 1999 *J. Colloid Interface Sci.* **210** 332
[3] Wette P, Schöpe H J and Palberg T 2005 *J. Chem. Phys.* **122** 144901
[4] Stipp A and Palberg T 2007 *Phil. Mag. Lett.* **87** 899
[5] Lorenz N, Liu J N and Palberg T 2008 *Colloids Surf.* A **319** 109
[6] Ivlev A V, Löwen H, Morfill G E and Royall C P 2012 *Complex plasmas and colloidal dispersions: particle-resolved studies of classical liquids and solids* (*Series in Soft Condensed Matter* vol 5) (Singapore: World Scientific)
[7] Emmerich H 2008 *Adv. Phys.* **57** 1
[8] Emmerich H, Löwen H, Wittkowski R, Gruhn T, Tóth G I, Tegze G and Gránásy L 2012 *Adv. Phys.* **61** 665
[9] Zahn K, Méndez-Alcaraz J M and Maret G 1997 *Phys. Rev. Lett.* **79** 175
[10] Pertsinidis A and Ling X S 2001 *Nature* **413** 147
[11] Zahn K and Maret G 1999 *Curr. Opin. Colloid Interface Sci.* **4** 60
[12] Dillmann P, Maret G and Keim P 2013 *Eur. Phys. J. Special Top.* **222** 2941
[13] Löwen H, Horn T, Neuhaus T and ten Hagen B 2013 *Eur. Phys. J. Special Top.* **222** 2961
[14] Deutschländer S *et al* 2013 *Eur. Phys. J. Special Top.* **222** 2973
[15] van Teeffelen S, Hoffmann N, Likos C N and Löwen H 2006 *Europhys. Lett.* **75** 583
[16] van Teeffelen S, Löwen H and Likos C N 2008 *J. Phys.: Condens. Matter* **20** 404217
[17] van Teeffelen S, Likos C N and Löwen H 2008 *Phys. Rev. Lett.* **100** 108302
[18] van Teeffelen S, Löwen H, Backofen R and Voigt A 2009 *Phys. Rev. E* **79** 051404
[19] van Teeffelen S, Achim C V and Löwen H 2013 *Phys. Rev. E* **87** 022306
[20] Hoffmann N, Ebert F, Likos C N, Löwen H and Maret G 2006 *Phys. Rev. Lett.* **97** 078301
[21] Ebert F, Keim P and Maret G 2008 *Eur. Phys. J.* E **26** 161
[22] Assoud L, Ebert F, Keim P, Messina R, Maret G and Löwen H 2009 *Phys. Rev. Lett.* **102** 238301
[23] Kollmann M, Hund R, Rinn B, Nägele G, Zahn K, König H, Maret G, Klein R and Dhont J K G 2002 *Europhys. Lett.* **58** 919
[24] König H, Hund R, Zahn K and Maret G 2005 *Eur. Phys. J.* E **18** 287
[25] Mazoyer S, Ebert F, Maret G and Keim P 2009 *Europhys. Lett.* **88** 66004
[26] Assoud L, Messina R and Löwen H 2007 *Europhys. Lett.* **80** 48001
[27] Fornleitner J, Lo Verso F, Kahl G and Likos C N 2008 *Soft Matter* **4** 480
[28] Hoffmann N, Likos C N and Löwen H 2006 *J. Phys.: Condens. Matter* **18** 10193
[29] Hansen J P and McDonald I 2006 *Theory of Simple Liquids* 3rd edn (Amsterdam: Academic)
[30] Talman J D 1978 *J. Comput. Phys.* **29** 35
[31] Heinen M, Allahyarov E and Löwen H 2014 *J. Comput. Chem.* **35** 275
[32] Assoud L, Ebert F, Keim P, Messina R, Maret G and Löwen H 2009 *J. Phys.: Condens. Matter* **21** 464114
[33] Singh Y 1991 *Phys. Rep.* **207** 351
[34] Löwen H 1994 *Phys. Rep.* **237** 249
[35] Wu J and Li Z 2007 *Ann. Rev. Phys. Chem.* **58** 85
[36] Roth R 2010 *J. Phys.: Condens. Matter* **22** 063102
[37] Smithline S J and Haymet A D J 1987 *J. Chem. Phys.* **86** 6486
[38] Barrat J L, Baus M and Hansen J P 1987 *J. Phys.* C **20** 1413
[39] Rick S W and Haymet A D J 1989 *J. Chem. Phys.* **90** 1188
[40] Denton A R and Ashcroft N W 1989 *Phys. Rev.* A **39** 4701
[41] Denton A R and Ashcroft N W 1990 *Phys. Rev.* A **42** 7312
[42] Denton A R and Ashcroft N W 1991 *Phys. Rev.* A **43** 3161
[43] Bolhuis P and Frenkel D 1994 *Phys. Rev. Lett.* **72** 2211
[44] Likos C N, Németh Z T and Löwen H 1994 *J. Phys.: Condens. Matter* **6** 10965
[45] Bolhuis P and Frenkel D 1997 *J. Phys.: Condens. Matter* **9** 381
[46] Denton A R and Löwen H 1997 *J. Phys.: Condens. Matter* **9** L1
[47] Xu H and Baus M 1990 *J. Phys.: Condens. Matter* **2** 5885
[48] Zeng X C, Oxtoby D W and Rosenfeld Y 1991 *Phys. Rev.* A **43** 2064
[49] Barrat J L, Baus M and Hansen J P 1986 *Phys. Rev. Lett.* **56** 1063
[50] Warshavsky V B and Song X 2008 *J. Chem. Phys.* **129** 034506
[51] Singh S P and Das S P 2007 *J. Chem. Phys.* **126** 064507
[52] Ramakrishnan T V and Yussouff M 1979 *Phys. Rev. B* **19** 2775

[53] Ballone P, Pastore G, Rovere M and Tosi M P 1985 *J. Phys. C: Solid State Phys.* **18** 4011

[54] Franzrahe K and Nielaba P 2009 *Phys. Rev. E* **79** 051505

[55] Marconi U M B and Tarazona P 1999 *J. Chem. Phys.* **110** 8032

[56] Archer A J and Evans R 2004 *J. Chem. Phys.* **121** 4246

[57] Español P and Löwen H 2009 *J. Chem. Phys.* **131** 244101

[58] Lichtner K, Archer A J and Klapp S H L 2012 *J. Chem. Phys.* **136** 024502

[59] Huang Z-F, Elder K R and Provatas N 2010 *Phys. Rev. E* **82** 021605

[60] Greenwood M, Ofori-Opoku N, Rottler J and Provatas N 2011 *Phys. Rev. B* **84** 064104

[61] Hansen-Goos H and Mecke K 2009 *Phys. Rev. Lett.* **102** 018302

[62] Wittmann R and Mecke K 2014 *J. Chem. Phys.* **140** 104703

[63] Marechal M, Goetzke H-H, Härtel A and Löwen H 2011 *J. Chem. Phys.* **135** 234510

[64] Marechal M, Zimmermann U and Löwen H 2012 *J. Chem. Phys.* **136** 144506

[65] Belli S, Dijkstra M and van Roij R 2012 *J. Chem. Phys.* **137** 124506

[66] Marechal M and Löwen H 2013 *Phys. Rev. Lett.* **110** 137801